2003-01-1450

Structure-Borne Noise Measures and Their Correlation to Sound Radiation over a Broad Range of Frequencies

Seungbo Kim and Rajendra Singh
The Ohio State University

ABSTRACT

Structure-borne noise within vehicle structures is often transmitted in a multi-dimensional manner and thus the vibro-acoustic model(s) of automotive powertrain or chassis must incorporate longitudinal and transverse (flexural) motions as well as their couplings. In this article, we employ the continuous system theory to model a typical vibration isolator (say the engine mounting system) and a compliant receiver that could simulate the body structure. The powertrain source is however assumed to be rigid, and both harmonic force and moment excitations are considered. Our analysis is limited to a linear time-invariant system, and the frequency domain based mobility method is utilized to synthesize the overall system. Contributions of both in-plane and flexural motions to structure-borne and radiated noise are incorporated. Two examples are considered to illustrate the methodology. First, multi-dimensional transmissibility and effectiveness terms are analytically and comparatively evaluated along with vibration power-based measures for an inverted 'L' beam receiver and selected source configurations. Further, free field sound pressures are calculated and correlated with structure-borne power transmitted to the receiver. Second, sound measurements and predictions for an experimental inverted 'L' plate receiver demonstrate that a rank order based on free field sound pressures may be regarded as a measure of structure-borne noise reduction. Measured insertion losses for sound pressure match well with those computed.

INTRODUCTION

Appropriate measures are necessary to properly assess structure-borne noise isolation and further to improve the isolation performance. For uni-directional motions, force and velocity transmissibility and related concepts are widely used [1]. Force or velocity effectiveness term, the ratio of transmitted force or velocity with an isolator to the one without the isolator, has also been employed [1, 2]. Those concepts are extended to a multi-dimensional problem [3, 4] but the incompatible units of off-diagonal terms hinder the further application of such measures [5]. For this reason, the concept of vibration power, with compatible units for both translational and rotational motions, has been used to assess transmission to receivers [6]. Power-based measures, such as input and transmitted powers and transmission efficiency, have also been studied for some infinite and finite structures [5, 6]. However, the quantification of structure-borne energy and source strengths still remain as key obstacles in many cases. Satisfactory resolution of such research issues would require appropriate structure-borne noise transmission measures. However, such measures for a multi-dimensional system are not well understood and often left to the discretion of user [1, 4]. Refer to our paper for further literature review [7].

In this article, we address this particular issue with emphasis on a multi-dimensional isolator in the presence of a compliant receiver. Problem is defined via Figure 1, in the context of source, path (isolator) and receiver. Formulations of our earlier articles are also utilized here such as the mobility synthesis formulation for prediction of overall system behavior [8], source characteristics [9] and Timoshenko beam solutions [5].

Chief objectives of this study include: 1. Examine alternate measures of vibration isolation performance for a multi-dimensional system and quantify the structure-borne noise transmission for several system configurations. 2. Calculate and measure the sound generated from the ‘L’ structure receiver and correlate results with vibration isolation measures. Key concepts will be illustrated via experimental and analytical studies on selected isolators.

VIBRATION ISOLATION MEASURES USING TRANSMISSIBILITY AND EFFECTIVENESS

SYSTEM WITH AN INVERTED ‘L’ BEAM RECEIVER: Various vibration isolation measures are examined for an analytical isolation system with an inverted ‘L’ beam

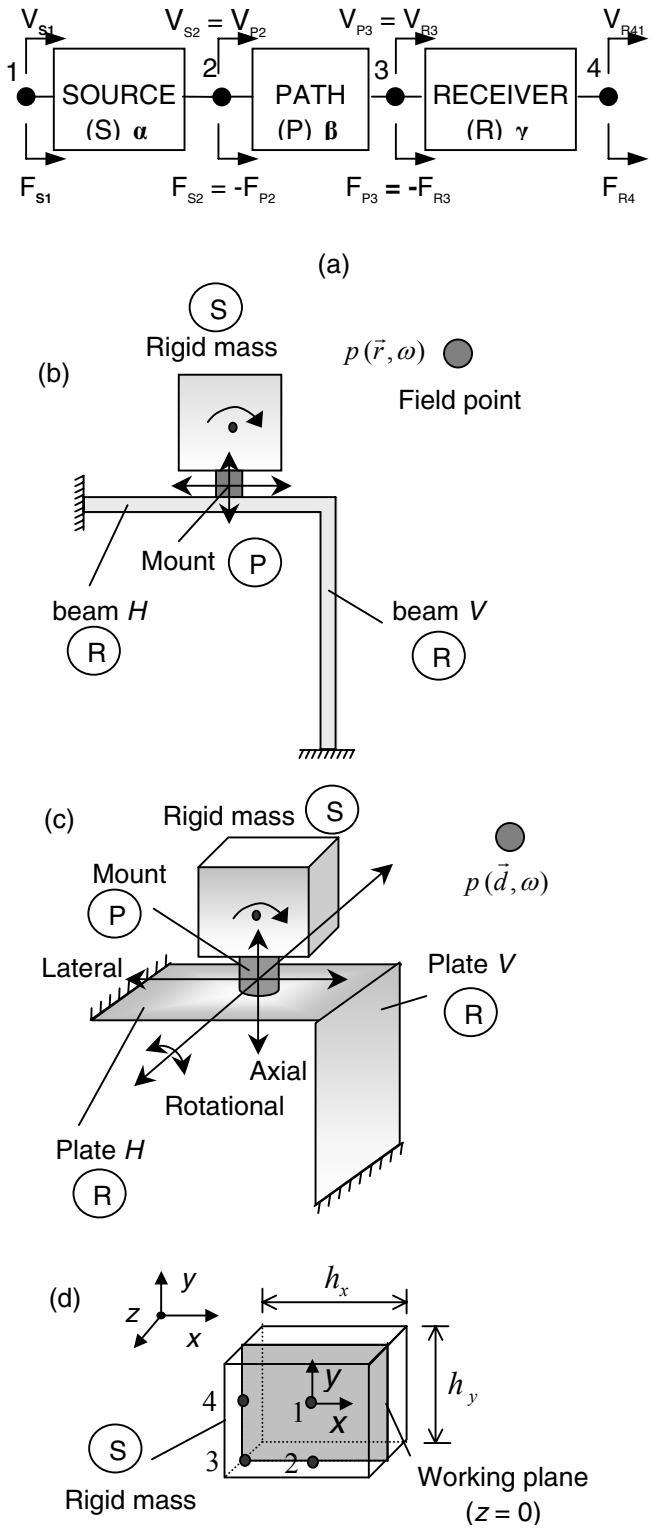

Figure 1. Configuration of the structure-borne noise isolation system. (a) Source-path-receiver system and their mobility matrices $\boldsymbol{\alpha}$, $\boldsymbol{\beta}$ and $\boldsymbol{\gamma}$. (b) system with an inverted 'L' beam receiver; (c) system with an inverted 'L' plate receiver; (d) isolator location [x, y, z] on the working plane of a cubic rigid body source: case 1 = [0, 0, 0]; case 2 = [0, $-h_y/2$, 0]; case 3 = [$-h_x/2$ $-h_y/2$, 0]; case 4 = [$-h_x/2$, 0, 0].

receiver of Figure 1(b). Note that longitudinal motion of one beam is coupled with flexural motion of the other and thus both contribute to sound radiation. The four isolator attachment cases of Figure 1(d) are analyzed up to 3 kHz. These cases provide several transmission configurations even though cases 3 and 4 are statically unstable and case 1 is physically meaningful only for three-dimensional motions in terms of its implementation. Nonetheless, vibration transmitted to the receiver is strongly affected by the mount location, and thus by the free velocity of source [9]. Harmonic moment excitations are applied at the mass center of source for vibratory power-based and sound field measures. Force excitation cases are also examined for transmissibility and effectiveness of force or velocity. The mobility matrix $\mathbf{M}$ of a rigid body, between any two locations i and j, can be determined from the inertia properties at mass center *G* and geometric information. Details may be found in reference [8]. The isolator is connected to the inverted 'L' beam at 0.75 ℓ_H where ℓ_H is the length of the horizontal beam. This off-center location highlights the effect of coupling mobility of receiver. Note that such a coupling mobility term does not exist for a centrally driven beam (with symmetric boundaries) and for an infinite beam. The circular cylindrical isolator is modeled using the Timoshenko beam theory to describe flexure along with the wave equation for longitudinal motion. Thus, the effects of shear deformation and rotary inertia are included. Mobilities of the Timoshenko beam have been analyzed for two types of solution in an earlier paper by the same authors [5]; the resulting formulations are used here. Material properties and dimensions of the source, isolator and the receiver beam are listed in Table 1.

Table 1. Material properties and dimensions of the analytical system of Figure 1(b).

Property or dimension	Source (Cubic rigid body)	Isolator (Circular beam)	Inverted 'L' beam Receiver
m (kg)	1	-	-
E (MPa)	-	16.2	6.688 X 10^4
G (MPa)	-	5	-
η	-	0.3	0.001
ρ (kg/m^3)	-	1000	2723
Dimensions in mm	ℓ = 50	ℓ = 30 *r* = 12	ℓ = 400 *b* = 100, *t* = 5 (horizontal and vertical beams)

VIBRATION ISOLATION MEASURES USING TR OR Ξ: The multi-dimensional force ($\mathbf{TR}_F$) and velocity ($\mathbf{TR}_V$) transmissibility matrices can be defined as follows where / represents a quotient operation for matrices and force and velocity vectors are defined in Figure 1(a):

$$\mathbf{TR}_F = \mathbf{F}_{R3}/\mathbf{F}_{S1}, \qquad \mathbf{TR}_V = \mathbf{V}_{R3}/\mathbf{V}_{S1}. \qquad \text{(1a-b)}$$

The effectiveness, the ratio of transmitted force or velocity with an isolator to the one without the isolator, matrices for force ($\mathbf{\Xi}_F$) and velocity ($\mathbf{\Xi}_V$) of a multi-dimensional system are also defined as follows:

$$\mathbf{\Xi}_F = \mathbf{F}_{3,\text{with}}/\mathbf{F}_{3,\text{without}}, \qquad \mathbf{\Xi}_V = \mathbf{V}_{3,\text{with}}/\mathbf{V}_{3,\text{without}}. \qquad \text{(2a-b)}$$

Here, subscripts "with" and "without" represent the interfacial force and response for system with and without any isolator respectively. Detailed mathematical formulations can be found in our earlier article [7].

Force and velocity transmissibilities (TR) are computed using the inverted 'L' beam receiver, with only one isolation configuration (case 2) of Figure 1(d). Only non-dimensional diagonal terms in transmissibility matrices are analyzed.

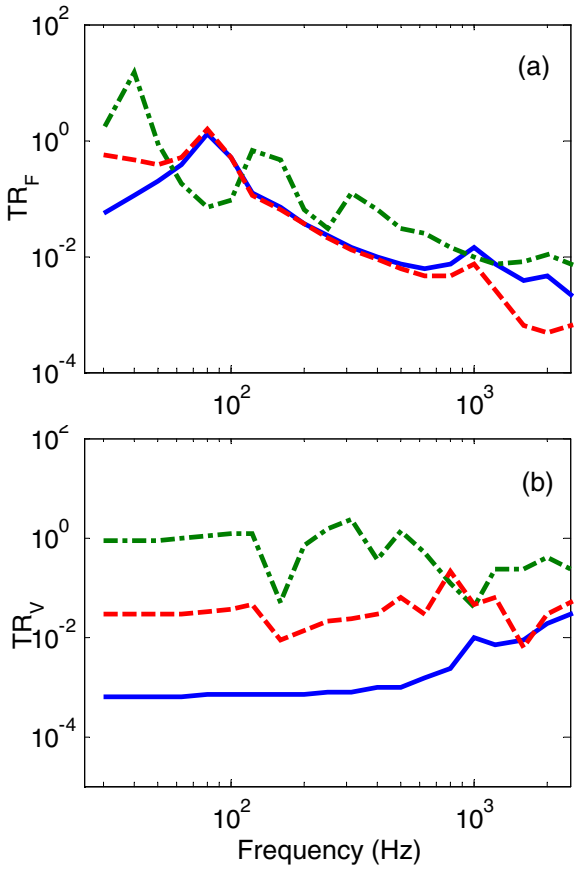

Figure 2. Transmissibility with an inverted 'L' beam receiver and case 2 isolator. (a) Force transmissibility TR_F; (b) velocity transmissibility TR_F. Key: ———, lateral (x); —·—·—·—, axial (y); - - - - - - - -, rotational (θ).

First, TR_F and TR_V spectra are shown in Figure 2. Spectral shapes and the rank order of TR_F are much different from the ones of TR_V. The lateral and rotational components of TR_F are almost the same over the entire frequency range and the axial TR_F is slightly higher than the others beyond 100 Hz. Unlike the TR_F, the axial component of TR_V dominates over the entire frequency range and the lateral component of TR_V is higher than the rotational component of those. Also, the differences between the TR_V components are more pronounced than the ones between the TR_F components. Further, the TR_F spectra decrease but the TR_V levels are maintained as frequency increases.

Next, the Ξ_F and Ξ_V effectiveness spectra are shown in Figure 3. Unlike the TR_V, the lateral and rotational components of Ξ_V are almost the same and the lateral component of Ξ_F is slightly larger than the rotational component of Ξ_F up to around 400 Hz, as shown in Figure 3. Therefore, the difference between TR_V and Ξ_V confirms that the TR_V does not properly represent the isolation effectiveness for the different motional directions, as known previously. However, similar to TR_V, it is observed that the axial component of Ξ_F or Ξ_V dominates beyond 100 Hz.

POWER-BASED VIBRATION ISOLATION MEASURES

The transmission efficiency Γ (a non-dimensional scalar quantity), the ratio of transmitted (to receiver) power Π_{TR} to input (to source) power Π_{IN}, is defined as follows:

$$\Gamma = \frac{\Pi_{\text{TR}}}{\Pi_{\text{IN}}}. \qquad (3)$$

Similarly, the effectiveness Ξ_Π of vibration power (a non-dimensional scalar quantity) can be defined as follows where "with" implies the net power transmitted to receiver with an isolator and "without" refers to the case when the source is rigidly connected to the receiver:

$$\Xi_\Pi = \frac{\Pi_{\text{TR, with}}}{\Pi_{\text{TR, without}}}. \qquad (4)$$

The four different cases of the isolator connection, as shown in Figures 1(d), are investigated using the same component parameters. Vibration power transmitted to receiver are computed and analyzed up to 3 kHz.

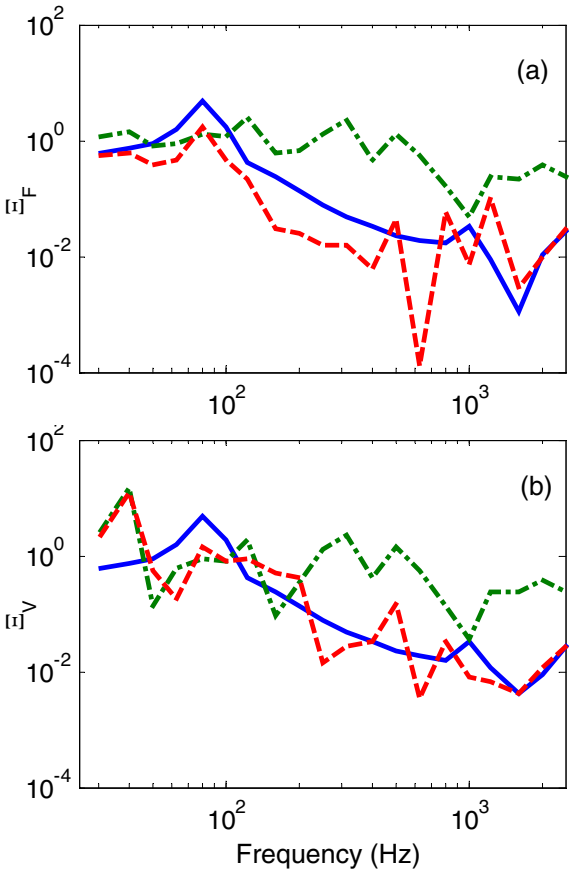

Figure 3. Effectiveness with an inverted 'L' beam receiver and case 2 isolator. (a) Force effectiveness Ξ_F; (b) velocity effectiveness Ξ_V. Key: ————, lateral (*x*); —·—·—·—, axial (*y*);- - - - - - - -, rotational (θ).

Total vibration powers Π_{Total} transmitted to the 'L' beam receiver are compared in Figure 4(a) for the 4 location cases of Figure 1(d) given unit (1 Nm) moment excitation. It is observed that total vibration powers for cases 3 and 4 are almost the same but these are higher than those for cases 1 and 2. Also, the transmitted power is lowest among the cases considered when the isolator is attached to mass center of rigid body (case 1). The power efficiencies Γ are shown in Figures 4(b), and a rank order based on Γ is similar to the one given by Π_{Total}. However, Γ in case 1 rises and is higher than the one for case 2 as ω increases. Also, for all cases, overall characteristics of Γ rise as ω increases even though the value of Π_{Total} decreases. The power effectivenesses Ξ_Π are also shown in Figure 4(c). The patterns for Ξ_Π spectra do not exactly match with Π_{Total} for the cases considered. For example, The Ξ_Π for case 3 is higher than the one of case 4 at low frequencies but is lower at high ω. Overall, one must properly select a power-based measure, given the choice between force (or velocity) transmissibility and effectiveness terms. Further, the differences between Π_{Total} and Γ are expected since the source input powers of each case are different although the excitation moment amplitude remains unchanged. Therefore, the source characteristics also need to be identified to examine various design modifications. For example, Γ is suitable when a source generating mechanism is clearly identified. Without a proper understanding of such a source, Π_{Total} must be evaluated for each design change.

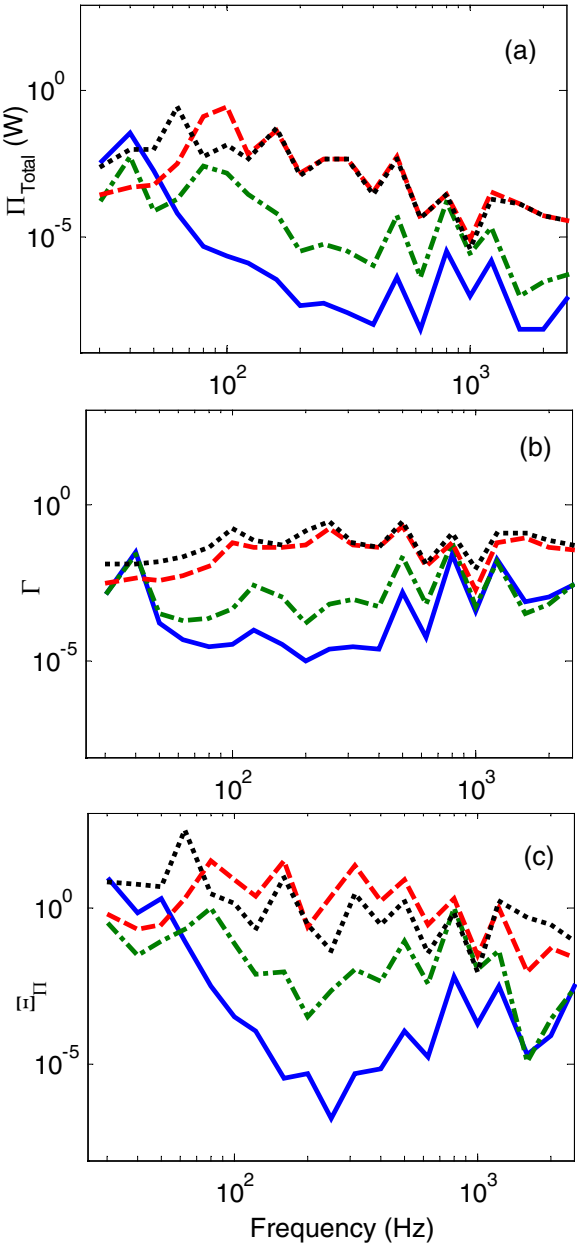

Figure 4. Power-based isolation measures with an inverted 'L' beam receiver given moment excitation. (a) Total transmitted vibration power Π_{Total}; (b) efficiency Γ for Π_{Total}; (c) effectiveness Ξ_Π for Π_{Total}. Key: ———— , mount location case 1; —·—·—·— , case 2; - - - - - - - -; case 3; ..... , case 4.

SOUND RADIATION FROM RECEIVER AS A MEASURE OF VIBRATION ISOLATION

Sound pressure *p* at selected points in free field ($\vec{d}$) is calculated in order to examine its relationship with vibration power transmitted to the receiver of Figure 1(b). An inverted 'L' beam is chosen as the chief radiating structure and it will incorporate contributions from longitudinal and flexural structural powers. See Figure 5 for more details of the system configuration. Also, a detailed derivation of the sound field radiated from the 'L' beam can be found in our earlier article [7]. Here, sound
field in the second quarter of Figure 5 is described by a superposition of two independent hemi-spherical spaces corresponding to the horizontal and vertical baffled beam radiators, as shown in Figure 5. Note that the Green's function for a ¾ free space is needed to describe the exact sound field and hence there may exist a discrepancy between the realistic sound field and the one described here especially at lower frequencies. Consequently, this study focuses on relative measures of two different systems, such as the insertion loss, and accordingly it is assumed that such discrepancies are negligible especially in the sound field located 45° from the corner of the beams. Yet, a more general case that employs an inverted 'L' plate and describes a 3-dimensional sound field is investigated via computational and experimental studies in a subsequent section of this article.

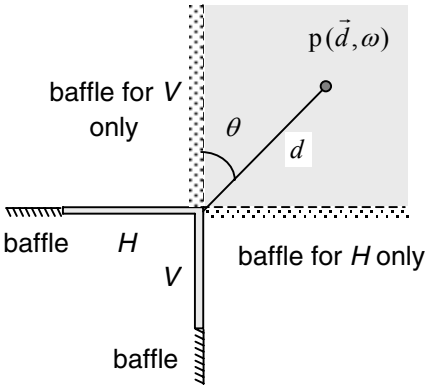

Figure 5. Sound radiation field from an inverted 'L' beam receiver.

Calculated mean-square sound pressures (Ψ_p^2) are shown in Figure 6 for four cases. Horizontal beam is connected to the isolator at $3\ell_H/4$ from its clamped end. The field point is located at *d* = 1 m from the intersection of two beams, at 45° from the outer surfaces of each beam, as shown in Figure 5. The rank order associated with four locations and related sound pressure spectral shapes of Figure 6 match the transmitted vibration power spectra of Figure 4(a) although some discrepancies are observed at some frequencies. Our calculation shows that the rank orders (corresponding to four isolator locations) at different sound field observation points do not change, except at some frequencies although their spectral shapes differ especially beyond 200 Hz. Refer to our article for results on sound pressures at other field locations [7].

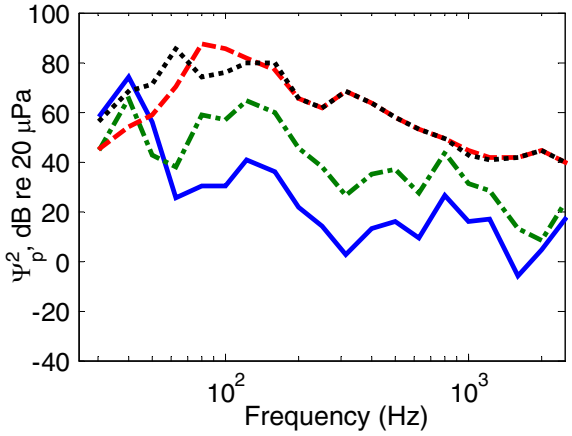

Figure 6. Far field sound pressures radiated by the 'L' beam of Figure 5 at a field location *d* = 1m, $\theta = 45^{\circ}$. Key: ————, mount location case 1; —·—·—·— , case 2; - - - - - - - -, case 3; ····· , case 4.

Figure 7 compares insertion losses based on mean-squared sound pressures ($IL_{\psi_p^2,i-j}$) at a field point with the ones of vibration power input ($IL_{\Pi,i-j}$) to the 'L' beam for four isolator cases of Figure 1(d) given the moment excitation. Here, subscripts *i* and *j* denote mount cases as shown in Figure 1(d).
Spectral averages of the insertion losses ($IL_{\psi_p^2,SAvg}$ and $IL_{\Pi,SAvg}$) are also compared in Figure 7. Figure 7 shows that the $IL_{\psi_p^2}$ spectra closely represent the IL_{Π} curves although some discrepancies between $IL_{\psi_p^2,4-1}$ and $IL_{\Pi,4-1}$ (cases 4 and 1) are observed. This suggests that $IL_{\psi_p^2,i-j}$ may not be equal to $IL_{\Pi,i-j}$ when systems *i* and *j* transmit different vibration components. Note that the rotational and axial components dominate the vibration transmission for cases 1 and 4 respectively. Therefore, in such cases, correlations between $IL_{\psi_p^2}$ and IL_{Π} could be enhanced by averaging sound pressures over the entire field.

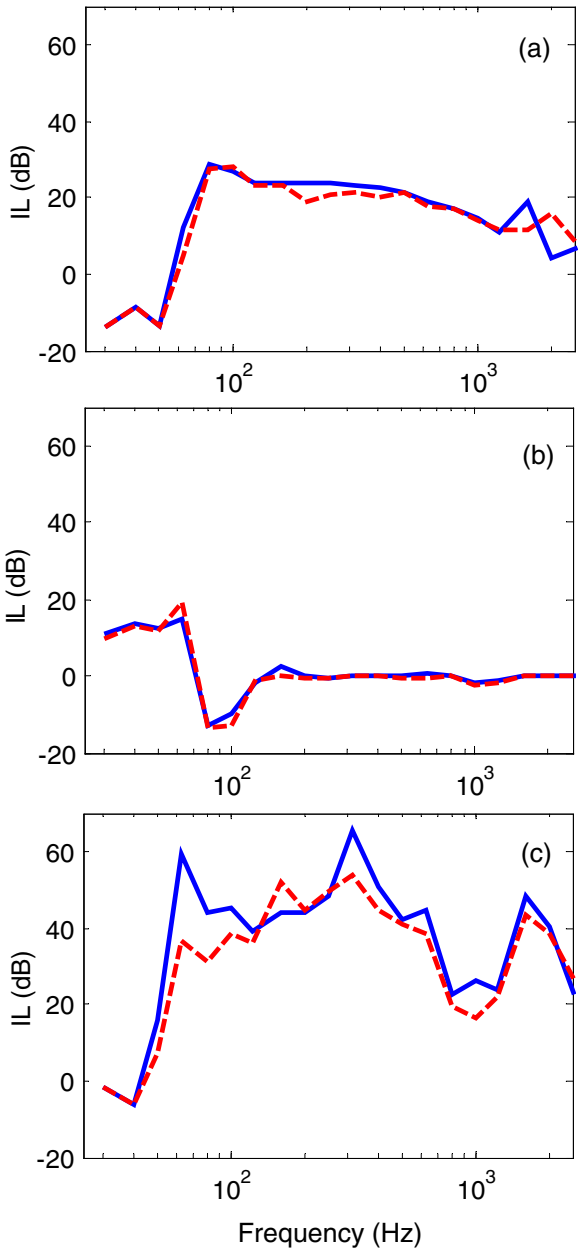

Figure 7. Insertion losses of mean square sound pressure ($IL_{\psi_p^2}$) and vibration power input (IL_{Π}) to the 'L' beam given moment excitation for four cases as shown in Figure 2(d). (a) $IL_{2\text{-}1}$ (case 2 - case 1) with spectral averages of $IL_{\psi_p^2,SAvg}$ = 14.3 dB, $IL_{\Pi,SAvg}$ = 13.5 dB; (b) $IL_{4\text{-}1}$ (case 4 - case 1) with $IL_{\psi_p^2,SAvg}$ = 35.9 dB, $IL_{\Pi,SAvg}$ = 31.5 dB; (c) $IL_{4\text{-}3}$ (case 4 - case 3) with $IL_{\psi_p^2,SAvg}$ = 1.0 dB, $IL_{\Pi,SAvg}$ = 1.4 dB. Key: ———, $IL_{\psi_p^2}$;--------, IL_{Π} . Here, subscript *SAvg* implies spectral average of corresponding insertion losses.

EXPERIMENTAL SYSTEM WITH AN INVERTED 'L' PLATE RECEIVER

SYSTEM CONFIGURATION: Similar to the inverted 'L' beam receiver, an inverted 'L' plate receiver, as shown in Figure 8, is employed to describe both in-plane and out-of plane motion transmissions to the receiver.

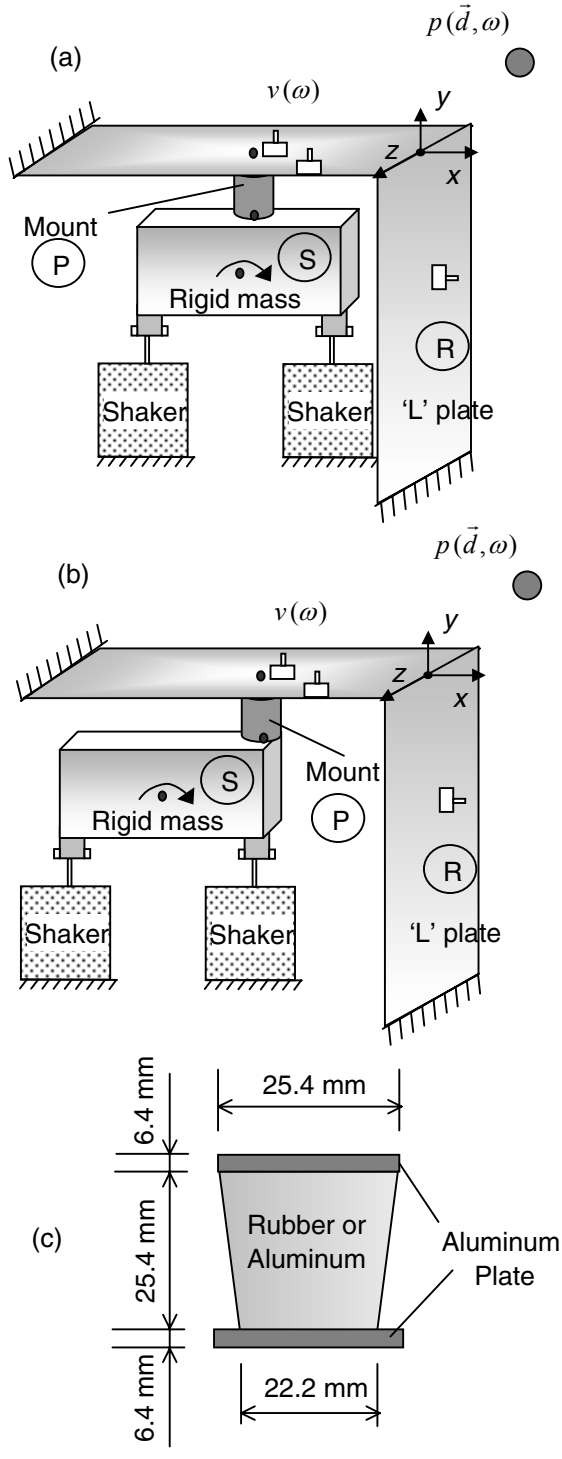

Figure 8. Experimental system with an inverted 'L' plate receiver, as excited by harmonic forces and moment. (a) System with rotational free velocity only; (b) system with translational and rotational free velocities; (c) isolator.

Mass and dimensions in x, y and z directions of rectangular rigid body are 1.2 kg, 140 mm, 64 mm and 47 mm respectively. Square (ℓ = 400, t = 1) steel (E = 19.5 x 10^4 N/m^2, ρ =7700 kg/m^3) plates are used for horizontal and vertical plates of the inverted 'L' plate receiver. Two different isolators (rubber or aluminum) of Figure 8(c) are experimentally studied. Each isolator is located at either the center or edge of mass to realize different vibration isolation configurations. However, the mount location on the receiver side is unchanged. The field point for sound pressure measurements $p(\omega)$ is located at a distance of 0.2 m from the mating edge of two plates, at 45º from the outer surfaces. Structural velocity at a selected point on the horizontal receiver plate is also examined. Measurement are conducted in an anechoic room under the sine sweep excitation (up to 3 kHz). In-phase and 180º out-of-phase forces (in y direction) are separately applied to the edges of the rigid source to simulate the force (f_y) and moment (q_z) excitations at G respectively. Forces from two shakers and accelerations at the driving point locations are measured using two impedance heads. Plastic and steel stingers are used over low (up to 1 kHz) and high (1 – 3 kHz) frequency regimes respectively since the dynamic forces could not excite the system above 1 kHz with plastic stingers. The input forces with almost the same magnitudes and 180º (or 0º) phase difference are maintained throughout the experiments for moment (or force) excitation cases. However, the phase between two forces deviates slightly from 180º (or 0º) at a system resonance (approximately 600 Hz). This resonance appears to be a result of the experimental system dynamics with two shakers. Forces measured at the driving point locations are used for computational predictions.

The mobilities of the inverted 'L' plate structure are obtained by using a commercial finite element (FEA) IDEAS [10] code. Further, interfacial forces and moments between the isolator and receiver are calculated by synthesizing the mobilities of the inverted 'L' plate, source and isolator. Then, the plate velocity distribution from FEA calculation is provided to a commercial boundary element method (BEM) SYSNOISE [11] code to predict the sound radiation. Individual sound fields generated by each plate for interfacial forces and moments are superimposed to determine the resultant sound pressure. Note that direct radiation from either source or isolator is not included in such calculations. Overall, sound pressure and velocity amplitudes are obtained using the FEA and BEM methods. Vibration power (Π_{TR}) transmitted to the 'L' plate and the power (Π_{RAD}) radiated to the acoustic medium from the receiver, as defined below, are also predicted:

$$\Pi_{\mathrm{RAD}} = \frac{1}{2}\int_A p\, v_a^*\, dS\,. \qquad (5)$$

Here, p and v_a are sound pressure and the particle velocity amplitudes respectively at a control surface S [6].

EFFECT OF ISOLATOR MATERIAL: The effect of isolator material properties is quantified in terms of insertion losses (IL) for sound pressure (p), vibration velocity (v) and acoustic power (Π_{RAD}) are calculated where

$$IL_{p_i} = 10\log_{10}\left(\frac{\Psi^2_{p_i,A}}{\Psi^2_{p_i,B}}\right),\ \mathrm{dB}; \qquad IL_{v_j} = 10\log_{10}\left(\frac{\Psi^2_{v_j,A}}{\Psi^2_{v_j,B}}\right),\ \mathrm{dB};$$

$$IL_{\Pi_{RAD}} = 10\log_{10}\left(\frac{\Pi_{RAD,A}}{\Pi_{RAD,B}}\right),\ \mathrm{dB}. \qquad (6a\text{-}c)$$

Here, p_i and v_j are sound pressure at acoustic field point i and velocity at receiver structure location j respectively. Further, 'A' and 'B' represent the system with an aluminum and rubber (or polypropylene) isolator respectively. The IL_p and IL_v spectra are obtained from both experimental and computational studies but only the computed results are used for $IL_{\Pi_{RAD}}$. The results are given at the center frequencies of the 1/3 octave band. The mount location is unchanged for all cases. Experimental and computational results are shown in Figure 9 when force (y) is applied at the mass center of a rigid body source. Further, the measured force inputs are used for computational studies. Resulting vibration and acoustic measures cannot be normalized with respect to their excitation forces since two different input forces are used. However, it is observed that measured input forces from the shaker stingers to a mass source do not vary much given different system configurations. Figure 9 shows that vibration and noise transmissions are much reduced over a wide range of frequencies when a rubber isolator with a lower G is used in place of an aluminum isolator. Further, $IL_{\Pi_{RAD}}$ spectra for sound power radiated from the 'L' plate receiver match well with the IL_p spectra for sound pressure, especially. However, the experiment results of IL_p do not exhibit as much reduction as the ones computed beyond 500 Hz. One of the reasons is that the actual sound radiated from the receiver is lower than shaker noise beyond 500 Hz, especially when a rubber isolator is located at the center of source. See Figure 9(b) where the background noise from shakers is also shown with mean-square sound pressure (Ψ^2_p). Note that measured Ψ^2_p of the system shows almost the same level as Ψ^2_p of shakers as shown in Figure 9(b). Further, note that IL_v spectra, that are not contaminated by shaker noise, are much

higher than IL_p beyond 500 Hz as shown in Figures 9(d). Observe that the IL_v from experiments reasonably match with predicted IL_v as shown in Figures 9(d). Spectral averages of measured and computed results are shown in Table 2 for insertion losses. Overall, reasonable agreements between computed and experimental results are observed even though some measurements are contaminated by the shaker noise.

EFFECT OF MOUNT LOCATION: The effects of mount location are examined using the experimental system of Figure 8. Only the rotational free velocity of the source should exist for the moment excitation case when a mount is located at the center of the mass source. And, both translational and rotational free velocities occur when the isolator is placed at the edge of the rigid body source [9]. Similar to the previous cases, insertion losses (*IL*) are calculated by using (6a-c). In this case, subscript '*A*' and '*B*' refer to the cases when the isolator is placed at the edge and at the center of the mass respectively. First, consider the rubber isolator case of Figures 10(a, c), where both computational and experimental results show that all vibration and sound measures are significantly reduced when an isolator is moved from the edge to the mass center. Like the previous case, measured IL_p spectra do not exhibit as much reduction as the ones computed beyond 500 Hz because the actual sound radiated from the receiver is lower than the shaker noise beyond 500 Hz, especially when a rubber isolator is located at the center of source. Further, similar to the previous case, IL_v spectra beyond 500 Hz are much higher than IL_p since measured IL_v are not contaminated by the shaker noise.

Next, aluminum isolator is examined. Figures 10(b, d) show that vibration and acoustic measures are reduced by connecting an aluminum mount at a source location with zero translational free velocity. However, the aluminum isolator case shows less reduction when compared to the rubber isolator case. Further, it is observed in Figures 10(b, d) that measured IL_p values exhibit a reasonable match with computed IL_p since the sound pressures with an aluminum mount are higher than the shaker noise level. Similar to the mount material case, spectral averages of the measured and computed insertion losses are again shown in Table 2. It is observed that significant reductions in vibration transmission, based on mount locations, are identified by using sound pressure measures for a system with a rubber isolator.

Velocity measure at a selected location also provides large reductions in vibration transmitted to a receiver. Like the previous case, reasonable agreements between computed and experimental results are observed even though some measurements are contaminated by the shaker noise as discussed before.

Table 2. Spectral averages of insertion losses for the experimental system of Figure 8.

Effect	Measure (Mean-square value)	Computation (dB)	Experiment (dB)
Isolator material given force excitation *	Velocity (Ψ_v^2)	8	7
	Sound pressure (Ψ_p^2)	15	10
Isolator location given moment excitation **	Velocity (Ψ_v^2)	22	20
		Rubber	
		7	11
		Aluminum	
	Sound pressure (Ψ_p^2)	21	15
		Rubber	
		7	7
		Aluminum	

Baseline for insertion loss calculation:
* system with Rubber isolator I
** system with a mount located at the center of the mass source

CONCLUSION

Several measures of vibration isolation performance have been critically examined for a multi-dimensional system with inverted 'L' structure receivers. Non-dimensional components of multi-dimensional transmissibilities and effectivenesses are comparatively evaluated for an inverted 'L' beam receiver and four source configurations. Radiated sound pressures resulting from both in-plane and out-of plane motions of the 'L' beam receiver, have also been calculated and correlated with power-based measures. Sound measurements and predictions for the inverted 'L' plate demonstrate that a rank order based on free field sound pressures, at one or more properly selected points, could be regarded as a measure of the vibration power transmitted to the receiver. Measured insertion losses for sound pressure match well with those based on

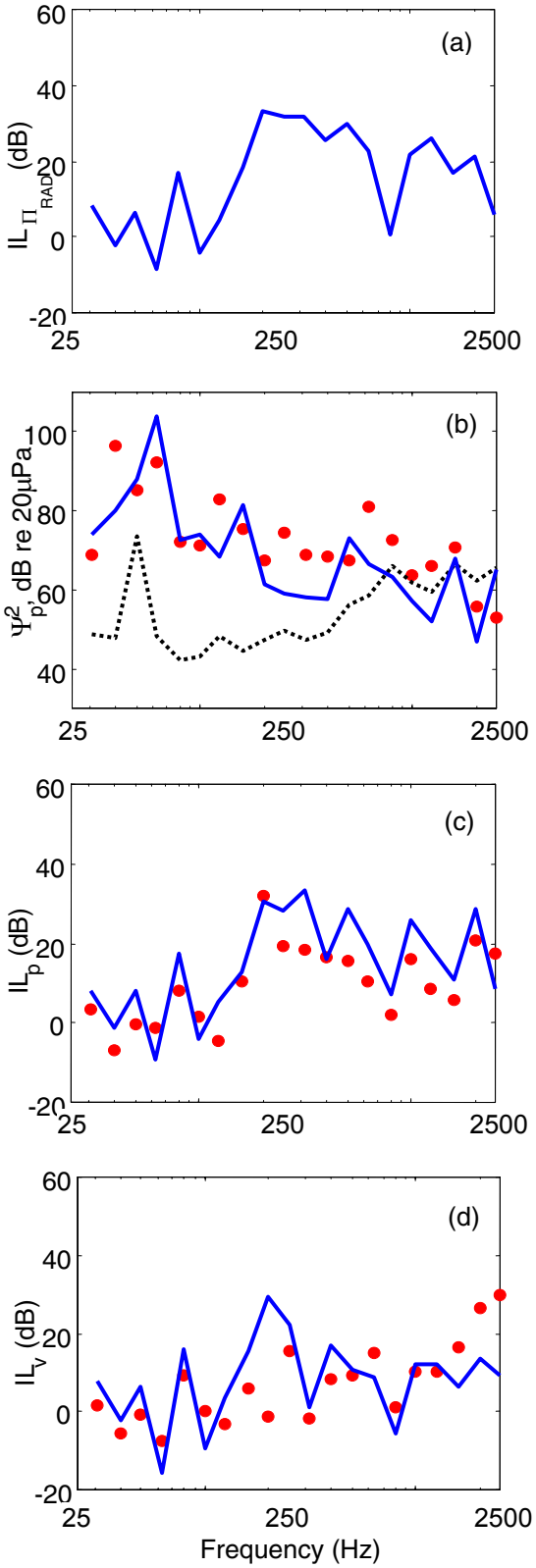

Figure 9. Vibration isolation measures on mount material effect given force excitation. (a) Insertion loss ($IL_{\Pi_{RAD}}$) of acoustic power radiated from the 'L' plate receiver; (b) mean-square sound pressure (Ψ_p^2); (c) insertion loss (IL_p) of sound pressure; (d) insertion loss (IL_v) of velocity. Key: ———, calculated; ● , measured; ·····, background noise from shakers.

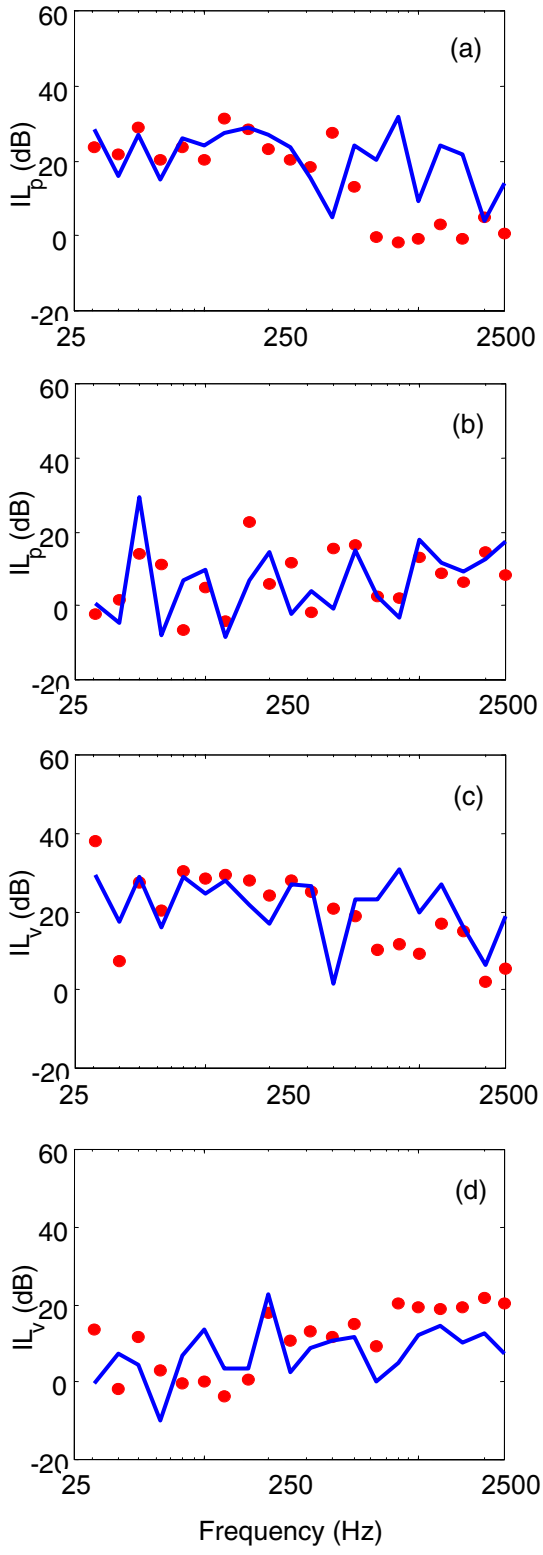

Figure 10. Insertion loss (IL) of sound pressure and velocity on mount location effect given moment excitation. (a) IL_p of sound pressure with rubber isolator; (b) IL_p of sound pressure with aluminum isolator; (c) IL_v of velocity with rubber isolator; (d) IL_v of velocity with aluminum isolator. Key: ———, calculated; ● , measured.

computed results, especially on the basis of spectrally-averaged values. The correlation found for the inverted 'L' plate structure, between transmitted power and sound radiation, suggests that such measures can be applied to evaluate automotive sub-systems such as the performance of powertrain mounting system.

ACKNOWLEDGMENTS

The General Motors Corporation (Noise and Vibration Center) and the Goodyear Tire and Rubber Company (Transportation Molded Products) are gratefully acknowledged for supporting this research.

REFERENCES

1. L. L. BERANEK 1988 *Noise and Vibration Control*. Washington, DC: Institute of Noise Control Engineering.
2. C. M. HARRIS 1987 *Shock and Vibration handbook*. New York: McGraw-Hill Book Company.
3. N. M. M. MAIA, J. M. M. SILVA and A. M. R. RIBEIRO 2001 *Mechanical Systems and Signal Processing*, 15(1), 129-137. The Transmissibility Concept in Multi-Degree-of-Freedom Systems.
4. D. A. SWANSON, L. R. MIILER and M. A. NORRIS 1994 *Journal of Aircraft*, 31(1), 188-196. Multidimensional Mount Effectiveness for Vibration Isolation.
5. S. KIM and R. SINGH 2001 *Journal of Sound and Vibration*, 248(5), 925-953. Vibration Transmission Through an Isolator Modeled by Continuous System Theory.
6. L. CREMER and M. HECKLE 1973 Structure-Borne Sound: Structural Vibrations and Sound Radiation at Audio Frequencies. New York: Springer-Verlag.
7. R. SINGH and S. KIM 2001 *Journal of Sound and Vibration*, Examination of Multi-Dimensional Vibration Isolation Measures and Their Correlation to Sound Radiation over a Broad Frequency Range (in press).
8. S. KIM and R. SINGH 2000 *Journal of Sound and Vibration*, 245(5), 877-913. Multi-Dimensional Characterization of Vibration Isolators over a Wide Range of Frequencies.
9. S. KIM and R. SINGH 2001 *Submitted to Journal of Sound and Vibration*, Source Characteristics of a Multi-Dimensional Vibration Isolation System.
10. I-DEAS *Users manual version 8.2.* 2000 SDRC, USA.
11. SYSNOISE Users manual version 5.4. 1999 NIT, Belgium.

LIST OF SYMBOLS

b	width
d	distance to sound observation point from reference
E	Young's modulus
$\mathbf{F}$	excitation vector
G	shear modulus
h	reference location in rigid body with respect to mass center
IL	insertion loss
ℓ	length
m	mass
p	sound pressure
r	radius
S	area
S, P, R	source, path and receiver
t	thickness
$\mathbf{TR}$	transmissibility matrix
$\mathbf{V}$	velocity vector
$\boldsymbol{\alpha}, \boldsymbol{\beta}, \boldsymbol{\gamma}$	mobility matrices of components
Γ	structural power efficiency
η	loss factor
$\boldsymbol{\Xi}$	effectiveness matrix
Π	vibration power (time-averaged)
ρ	mass density
Ψ	mean-square
ω	frequency, rad/sec

Subscripts

H	horizontal beam or plate
IN	input
RAD	radiated
S, P, R	source, path and receiver
$SAvg$	spectral average
TR	transmitted out
V	vertical beam or plate
with	with isolator
without	without isolator
x, y, z	cartesian coordinates
1, 2, 3, 4	reference locations

Operators

/	quotient for matrices

CONTACT

http://rclsgi.eng.ohio-state.edu/~singh/ADL.html